ACS OMEGA

Open Access

http://pubs.acs.org/journal/acsodf

Article

Thr-to-Ala Mutation Leads to a Larger Aromatic Pair and Reduced Packing Density in α1,α3-Helices during Thioredoxin Cold Adaptation

Tu Anh Nguyen and ChangWoo Lee*

Cite This: *ACS Omega* 2024, 9, 10812−10824

Read Online

ACCESS | Metrics & More | Article Recommendations | Supporting Information

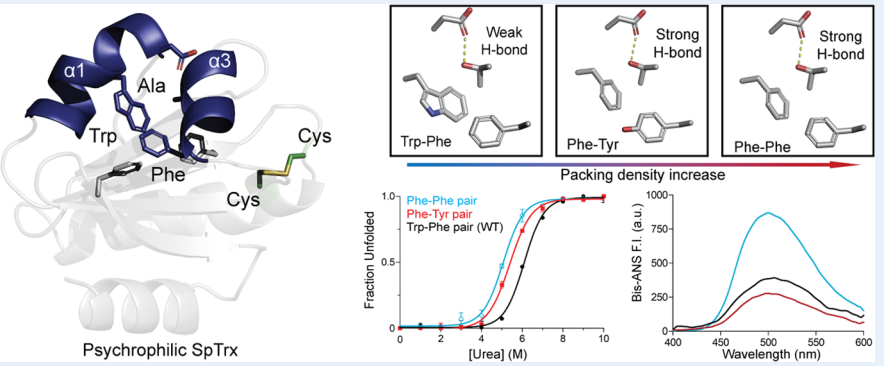

ABSTRACT: This study investigates the impact of aromatic−aromatic interactions on the cold adaptation of thioredoxin (Trx), a small redox protein with a conserved Trx-fold structure. Two Trx orthologs, one from the psychrophilic Arctic bacterium *Sphingomonas* sp. (SpTrx) and the other from the mesophilic *Escherichia coli* (EcTrx), display distinct aromatic interactions in their α1,α3-helices. SpTrx features a larger Trp11-Phe69 pair, while EcTrx employs a smaller Phe12-Tyr70 pair along with an additional Asp9-Thr66 hydrogen bond. Smaller aromatic residues in SpTrx (Phe-Phe or Phe-Tyr pair) lead to decreased thermal and thermodynamic stabilities, increased conformational flexibility, and reduced enzyme activity. In contrast, EcTrx's thermal stability is primarily influenced by the larger Trp residue, especially in the more hydrophobic Trp-Phe pair compared to the Trp-Tyr pair. Both SpTrx and EcTrx exhibit a strengthening of the Asp-Thr hydrogen bond by a Phe-Tyr pair and a weakening by a Trp-Phe pair. Additionally, the Asp8-Thr65 hydrogen bond in SpTrx contributes to the destabilization of the Phe-Phe pair. Molecular dynamics simulations of SpTrx indicate that a smaller aromatic pair or the Asp-Thr hydrogen bond in the α1,α3-helices further destabilizes the α2-helix across the central β-sheet. Our results suggest that the Thr-to-Ala mutation destabilizes the α1,α3-helices, resulting in a larger aromatic pair and reduced packing density in psychrophilic Trxs during cold adaptation. These findings enhance our understanding of Trx's adaptation to colder temperatures.

1. INTRODUCTION

Trx is a small redox protein (∼12 kDa) with a conserved Trx-fold consisting of five β-strands and four flanking α-helices.[1] Trx has the redox-active WCXXC catalytic motif,[2,3] which is critical for regulating the cellular redox state, preventing oxidative stress, and maintaining proper cell function.[4−6] Trx-S_2, the oxidized form, receives electrons from NADPH via Trx reductase and transfers them to various cellular reductases through disulfide exchange.[5,6]

The Trx-fold, conserved for four billion years, exhibits high thermal and thermodynamic stabilities.[6−9] Trxs can withstand denaturation temperatures up to 123 °C,[10] due to the rigidity of their hydrophobic core, encompassing both the central β-sheets[11−14] and the C-terminal α4-helix with the rest of the protein.[14,15] However, Trxs from mesophiles and psychrophiles typically display lower thermal stability than their thermophilic counterparts.[7,16−19] The short α3-helix is a part of the substrate binding region, and changes in its dynamics significantly influence the protein's catalytic activity.[20,21] Furthermore, mutations enhancing protein stability primarily locate on the α3-helix,[10,22] where short-range polar interactions play a more significant role than long-range interactions.[23] Studies using the dynamic flexibility index showed that during the evolution from hyperthermophilic to mesophilic Trxs, increased flexibility in the α3-helix correlated with a decrease

Received: December 7, 2023
Revised: January 18, 2024
Accepted: February 8, 2024
Published: February 24, 2024

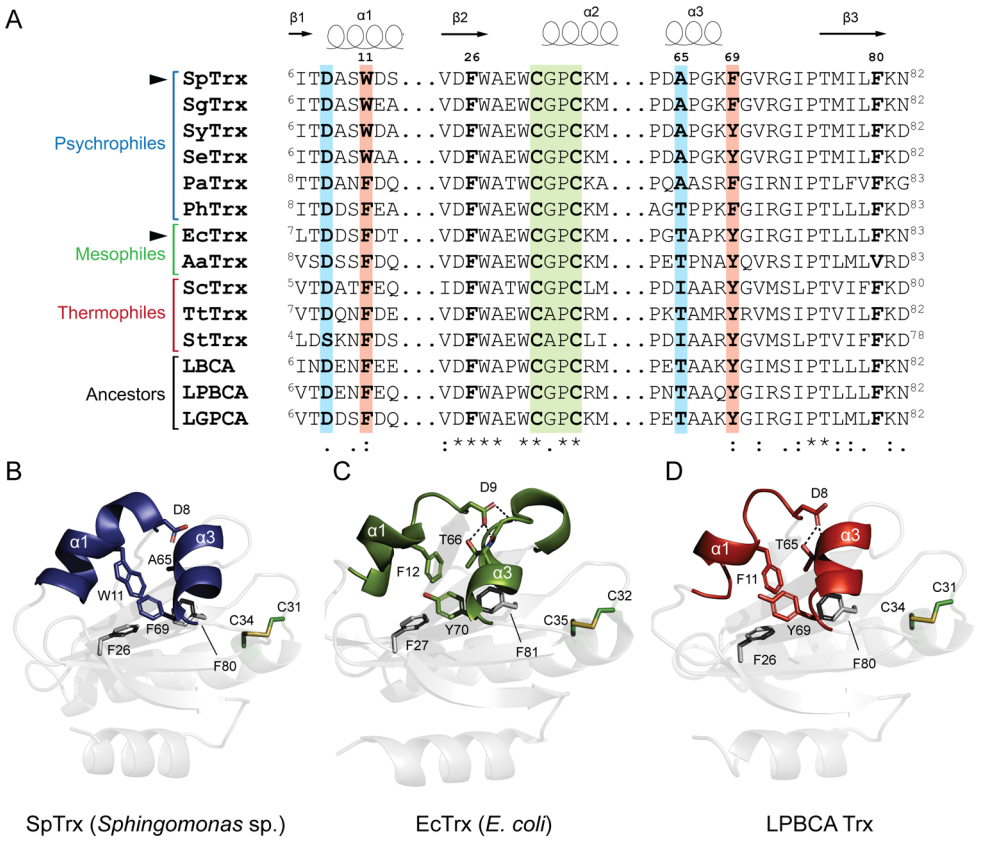

Figure 1. Amino acid sequence and structural comparison of Trxs. (A) Multiple sequence alignment of Trxs adapted to different habitat temperatures: Trxs from psychrophiles: SpTrx (*Sphingomonas* sp. PAMC 26621, NCBI ID: WP_010164143.1), SgTrx (*Sphingomonas* sp., NCBI ID: WP_133186775.1), SyTrx (*Sphingomonas psychrolutea*, NCBI ID: WP_188445499.1), SeTrx (*Sphingomonas echinoides*, NCBI ID WP_010402847.1), PaTrx (*Psychrobacter arcticus*, NCBI ID: WP_011281244.1), PhTrx (*Pseudoalteromonas haloplanktis* TAC 125, NCBI ID: WP_008109071.1); Trxs from mesophiles: EcTrx (*Escherichia coli*, PDB ID: 2TRX), AaTrx (*Acetobacter aceti*, PDB ID: 2I4A); Trxs from thermophiles: ScTrx (*Streptococcus* sp., NCBI ID: WP_002884315.1), TtTrx (*Thermus thermophilus*, PDB ID: 2CVK), StTrx (*Sulfolobus tokodaii*, PDB ID: 2E0Q); Ancestral Trxs: LBCA (Last Bacteria Common Ancestor, PDB ID: 4BA7), LPBCA (Last Common Ancestor of Cyanobacterial, *Deinococcus*, and *Thermus* group, PDB ID: 2YJ7), and LGPCA (Last γ-Proteobacteria Common Ancestor, PDB ID: 2YN1). Right-pointing triangles indicate the target proteins investigated in this study. The catalytic motif is depicted in green, while the highly conserved Asp8 and Ala65 are highlighted in blue. Aromatic pairs in α1,α3-helices are marked in orange, and the aromatic cluster, comprising Trp11, Phe26, Phe69, and Phe80 (SpTrx numbering), is shown in bold. (B–D) Comparison of α1,α3-helix interactions among the AlphaFold predicted model of SpTrx, as well as the crystal structures of EcTrx (PDB ID: 2TRX), and LPBCA Trx (PDB ID: 2YJ7), respectively.

in protein melting temperature (T_m).[24,25] These observations suggest the α3-helix's role in regulating the protein's overall flexibility and thermal stability.

Trx's hydrophobic core consists of two clusters: aliphatic and aromatic.[2] The aromatic cluster, characterized by a tetrahedral arrangement, includes two highly conserved Phe residues on the β2 and β4-strands,[11,12] as well as two variable aromatic residues at the contact between α1 and α3-helices (Figure 1A). The identity of these residues varies depending on the habitat temperature. In ancestral, thermophilic, and mesophilic Trxs, it is common to find a smaller Phe-Tyr pair at these positions. However, psychrophilic Trxs exhibit distinct aromatic pairs, with many featuring larger Trp-Phe or Trp-Tyr pairs, while a minority features a smaller Phe-Phe pair (Figure 1B). Interestingly, Trx orthologs with smaller aromatic pairs in the α1,α3-helices are characterized by an adjacent Asp-Thr hydrogen bond, unlike orthologs with larger aromatic pairs (Figure 1C,D). Furthermore, the presence of Ile, corresponding to Thr66 in EcTrx, in thermophilic and mesophilic Trxs (Figure 1A) emphasizes its role in Trx's temperature adaptation through hydrophobic interactions.

This study investigates the role of pairwise aromatic interactions and hydrogen bonds between α1 and α3-helices in Trx cold adaptation. We focus on two Trx orthologs: SpTrx from the Arctic bacterium *Sphingomonas* sp. PAMC 26621, which features a Trp11-Phe69 pair, and EcTrx from mesophilic *E. coli*, characterized by a Phe12-Tyr70 pair. To explore their roles, we introduced smaller aromatic pairs (Phe-Phe and Phe-Tyr) into SpTrx (W11F and W11F/F69Y), while also establishing an Asp8-Thr65 hydrogen bond (A65T, W11F/A65T, and W11F/A65T/F69Y). For comparison, counterpart mutations were introduced in EcTrx, including the Trp-Tyr pair (F12W), Trp-Phe pair (F12W/Y70F), and Phe-Phe pair (Y70F). We also examined the role of the Asp9-Thr66 hydrogen bond in EcTrx in combination with three different aromatic pairs: Phe-Tyr (T66A), Phe-Phe (T66A/Y70F), and Trp-Phe (F12W/T66A/Y70F). Through this study, we demonstrate the crucial role of specific aromatic pairs and the proximity of Thr in Trx's adaptation to cold temperatures, providing insights into its cold adaptation mechanism.

https://doi.org/10.1021/acsomega.3c09806
ACS Omega 2024, 9, 10812−10824

2. MATERIALS AND METHODS

2.1. Materials. *Sphingomonas* sp. PAMC 26621 was provided by the Polar and Alpine Microbial Collection of the Korea Polar Research Institute (Incheon, South Korea).[26] The *ectrx* gene in the pET32 expression vector was obtained from Addgene (Watertown, MA). The pET28(+) expression vector was acquired from Novagen (Madison, WI). The *n*Pfu-Forte polymerase and Dpn I were obtained from Enzynomics (Daejeon, South Korea). HisTrap and Capto Q columns were purchased from GE Healthcare (Piscataway, NJ). Bis-ANS was purchased from Invitrogen (Waltham, MA). DTNB (Ellman's Reagent) was purchased from ThermoFisher Scientific (Waltham, MA). All other chemical reagents were purchased from Sigma (St. Louis, MO) or Tokyo Chemical Industry (Tokyo, Japan) unless stated otherwise.

2.2. Structural Analysis and Multiple Sequence Alignment. BLAST searches were conducted against the National Center for Biotechnology Information (https://www.ncbi.nlm.nih.gov/) and Protein Data Bank (https://www.rcsb.org/) using the amino acid sequence of SpTrx as a template. The amino acid sequence identities of SpTrx to EcTrx and LPBCA (Last Common Ancestor of Cyanobacterial, *Deinococcus*, and *Thermus* group) Trx are 62 and 45%, respectively. The structural models of SpTrx WT and mutants were constructed using AlphaFold,[27] achieving high pLDDT scores (the predicted local distance difference test) ranging from 92 to 96. The crystal structures of EcTrx[3] and LPBCA Trx[28] were visualized by PyMOL (The PyMOL Molecular Graphics System, Version 2.0 Schrödinger, LLC.). Multiple sequence alignment of Trx orthologs was performed using Clustal Omega.[29] The distance of aromatic−aromatic interactions ($\pi-\pi$ stacking) was calculated using the Protein Interaction Calculator (PIC) server.[30] The packing density was calculated using the ProteinVolume tool.[31]

2.3. Site-Directed Mutagenesis. Site-directed mutagenesis using *n*Pfu-Forte polymerase was employed to create mutations in the *sptrx* and *ectrx* genes in pET28(+) and pET32 vectors, respectively, with PCR primers listed in Table S1. The double mutants (SpTrx W11F/A65T and W11F/F69Y) were generated by substituting Thr for Ala65 and Tyr for Phe69 in SpTrx W11F, respectively. The triple mutation W11F/A65T/F69Y was created by replacing Ala65 with Thr in the W11F/F69Y background. In the case of EcTrx, the double mutants (EcTrx F12W/Y70F and EcTrx T66A/Y70F) were formed by substituting F12W and T66A into EcTrx Y70F, respectively. The triple mutation EcTrx F12W/T66A/Y70F was generated by replacing Thr66 with Ala using EcTrx F12W/Y70F as a template. Following PCR amplification, the products were treated with Dpn I at 37 °C for 1 h before being transformed into *E. coli* BL21 (DE3). The accuracy of the mutant plasmids was confirmed through DNA sequencing.

2.4. Expression and Purification of SpTrx WT and Mutant Proteins. A single colony of *E. coli* BL21 (DE3) was grown overnight in a Luria−Bertani (LB) medium with 100 μg/mL kanamycin or ampicillin. The overnight culture was inoculated into a 200 mL LB medium. 1 mM IPTG was added to the LB medium upon reaching an optical density of 0.6−0.8 at 37 °C, and the culture was grown for an additional 6 h at 30 °C. The cells were harvested by centrifugation and then resuspended in buffer A (50 mM Tris·HCl, pH 8.0, 50 mM NaCl, 5 mM imidazole, and 0.1 mM EDTA), followed by sonication on ice. The supernatant was loaded into a 1 mL HisTrap column equilibrated with buffer A. The recombinant Trx proteins were eluted with a linear gradient of 20−300 mM imidazole in buffer A. Proteins in elution fraction were loaded into a 5 mL Capto Q column on an AKTA go system (GE Healthcare). The proteins were then eluted with a linear gradient of 50−1000 mM NaCl in buffer B (50 mM Tris·HCl, pH 8.0, and 50 mM NaCl). All fractions containing the target proteins were pooled. The purified proteins were kept in buffer B with 5% glycerol and stored at −80 °C for further experiments.

2.5. Temperature-Induced Unfolding and Thermal Reversibility. Temperature-induced unfolding and thermal reversibility measurements were conducted using a Scinco FS-2 fluorescence spectrometer (Seoul, South Korea) with an excitation wavelength of 280 nm (emission measured between 300 and 400 nm). Proteins were equilibrated in buffer C (50 mM potassium phosphate, pH 7.5, and 50 mM NaCl) using a 10 kDa cutoff column, with a sample concentration of 1 μM. The fluorescence of the protein at 4 °C was measured to identify its native conformation. Unfolding of the protein was monitored over the temperature range of 50−90 °C, with 10 °C increments and 30 min equilibration at each point. For refolding, the protein was initially incubated at 90 °C, then gradually cooled from 60 to 30 °C in steps of 10 °C with a 30 min equilibration period. Background correction was performed by subtracting the buffer values at corresponding temperatures, and fluorescence spectra were smoothed using Origin Pro software (Northampton, MA). Fractional unfolding was calculated and analyzed with GraphPad Prism software (San Diego, CA).

2.6. Protein Thermal Shift Analysis. A thermal shift assay using SYPRO orange dye was conducted on an Applied Biosystems StepOne Plus Real-Time PCR instrument (ThermoFisher Scientific) using continuous ramp mode at 1% ramp rate per sec from 25 °C through 99 °C. The final protein concentration (0.3 mg/mL) was mixed with buffer D (100 mM sodium phosphate, pH 7.2, and 100 mM NaCl) containing 3× SYPRO orange dye, resulting in a total volume of 20 μL. The melting temperature (T_m value), at which 50% of the protein was denatured, was determined using Protein Thermal Shift software v1.4 (Applied Biosystems).

2.7. Fluorescence Spectroscopy. Intrinsic protein fluorescence measurements were conducted to access urea-induced protein unfolding, and acrylamide quenching of protein fluorescence using a Scinco FS-2 fluorescence spectrometer. The excitation wavelength was set at 280 nm and emission was measured in the range of 300−400 nm. For urea-induced protein unfolding, 10 μM SpTrx WT and mutants were incubated for 30 min with urea (0−10 M) in buffer E (50 mM potassium phosphate, pH 7.5) at 25 °C. The equilibrium constant (K_{eq}) was then used to determine Gibbs free energy ($\Delta G^0_{H_2O}$) using eq 1[32]

$$\Delta G^0_{H_2O} = -RT\ln(K_{eq}) \quad (1)$$

where R represents the gas constant in J K^{-1} mol^{-1} and T is the temperature in Kelvin (K). A plot of ΔG as a function of the urea molarity follows a linear relationship.

Protein fluorescence measurements were conducted to evaluate acrylamide-induced quenching. 10 μM proteins were separately incubated at 4 and 50 °C for 2 h in buffer B. After incubation, acrylamide concentrations ranging from 0 to 0.5 M were added to buffer B for 2 min at 25 °C, and fluorescence

https://doi.org/10.1021/acsomega.3c09806
ACS Omega 2024, 9, 10812−10824

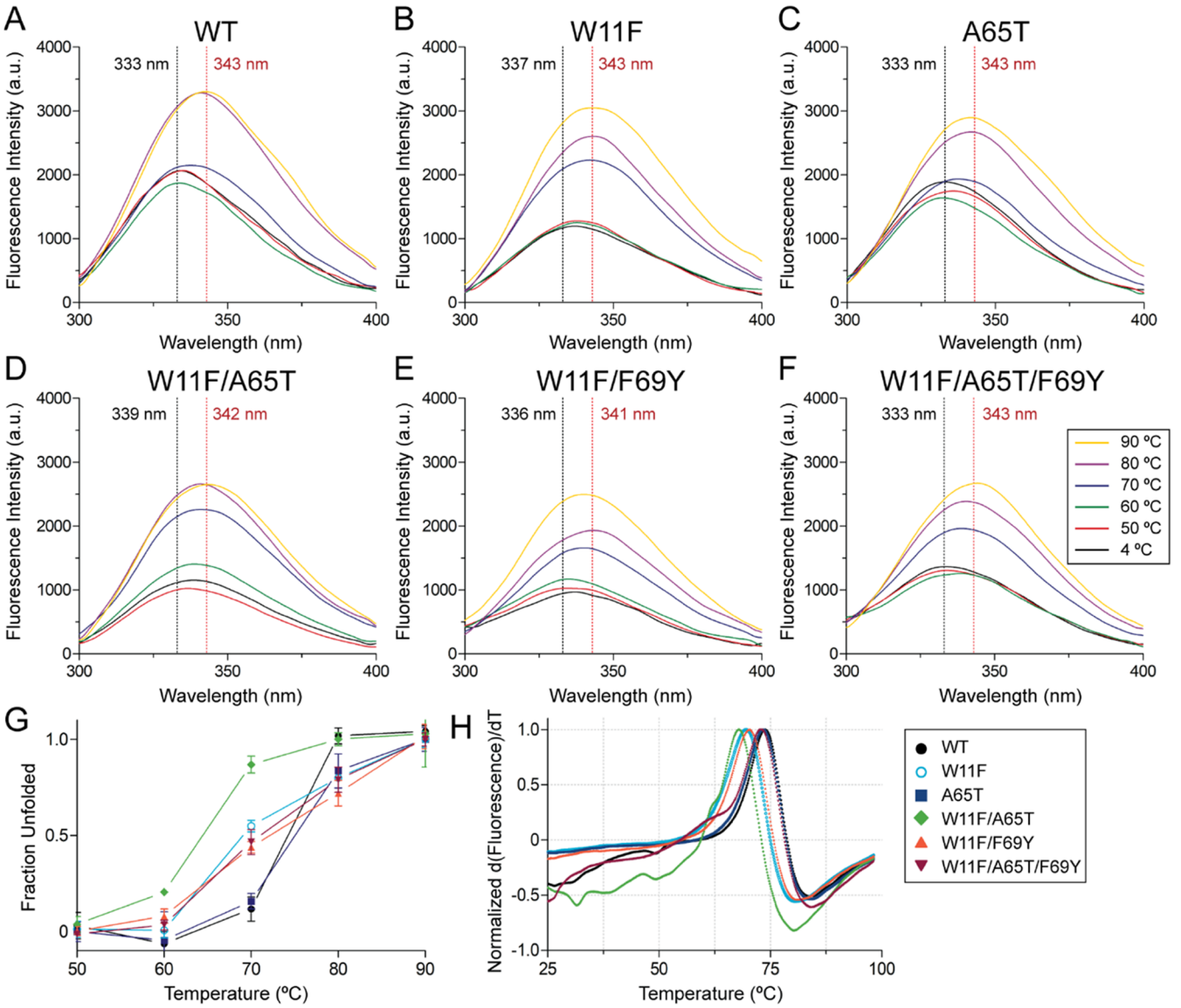

Figure 2. Thermal stability profile of SpTrx WT and mutants. (A−F) Temperature-induced protein unfolding. The intrinsic fluorescence of protein was recorded at temperatures of 4 °C (black), 50 °C (red), 60 °C (green), 70 °C (blue), 80 °C (purple), and 90 °C (yellow) with 30 min intervals during heating. Maximum wavelengths (λ_{max}) of native and unfolded protein were marked in black and red dash-line, respectively. (G) Fraction of unfolded proteins plotted against temperature. Fluorescence intensities between temperatures are presented as the ratio of the maximum fluorescence at 4 °C (F_0) to those at other temperatures (50, 60, 70, 80, and 90 °C). (H) Thermal denaturation curve of SpTrx proteins. Thermal denaturation curve of proteins was determined using real-time PCR system with SYPRO Orange-based thermal shift analysis. The maximum fluorescence intensity of each protein was set as 1. Data presented are the mean ± SD of at least three independent biological replicates.

was measured. Acrylamide Stern−Volmer plots were generated by plotting the ratio of intrinsic fluorescence intensity (F_0) to fluorescence intensity (F) in the presence of 0−0.5 M acrylamide. The resulting plots displayed a slight upward curve when F_0/F was plotted against [Q]. The modified Stern−Volmer equation was used eq 2[33]

$$F_0/F = 1 + K_{SV}[Q] \quad (2)$$

where Q represents acrylamide concentration and K_{SV} is the Stern−Volmer constant calculated from the quenching curve's slope.

The tertiary structure changes of SpTrx WT, W11F, and W11F/F69Y were assessed using bis-ANS fluorescence. 10 μM proteins in buffer B were incubated at 4 and 50 °C for 2 h before being added to the reaction mixture containing 100 μM bis-ANS in buffer B, respectively. Following 30 min incubation, the fluorescence spectra of the samples were detected at 25 °C (excitation at 385 nm and emission at 400−600 nm).

2.8. Limited Proteolysis. SpTrx WT and mutants underwent proteolytic digestion using trypsin and proteinase K (Sigma) in buffer F (50 mM sodium phosphate, pH 7.0, and 0.5 mM $CaCl_2$) at 25 °C for 30 min. Each reaction consisted of 60 μg protein and 1 μg trypsin (or 15 ng proteinase K). The digestion was stopped by adding 5× SDS sample buffer containing 5.2 mM PMSF and 5.2 mM EDTA, followed by boiling at 100 °C for 3 min. The resulting mixture was loaded onto a tricine-SDS-polyacrylamide gel to separate proteins smaller than 30 kDa.[34] After electrophoresis, the gels were stained with Coomassie Blue and subsequently destained. The intensity of native bands was analyzed using ImageJ software.[35]

https://doi.org/10.1021/acsomega.3c09806
ACS Omega 2024, 9, 10812−10824

2.9. Far-UV Circular Dichroism (CD) Spectroscopy. The proteins at a final concentration of 0.38 mg/mL in buffer B were incubated at 25 °C. The CD spectra were measured using a JASCO J-1500 spectropolarimeter at the Center for Scientific Instruments, Kyungpook National University (Daegu, Korea). The results show residual ellipticity (mdeg) versus wavelength using GraphPad Prism software. The α-helical, β-sheet, turn, and random coil content of each protein was determined using the BeStSel server.[36]

2.10. Insulin Reduction Assay Using SpTrx WT and Mutants. Insulin (0.13 mM) and SpTrx proteins (14.6 μM) were added to the reaction mixture (100 mM sodium phosphate, pH 7.0, 2 mM EDTA, and 0.33 mM DTT), resulting in a final volume of 800 μL. A negative control without the Trx protein was also included. The mixtures were incubated at 25 °C and measured at 5 min intervals for up to 50 min using a Shimadzu UV-1800 spectrophotometer (Kyoto, Japan) to measure the absorbance of the precipitated β-chain of Insulin at 650 nm. The initiation time of precipitation was determined as the point where the absorbance at 650 nm increased by 0.02 over a stable baseline recording. The rate of precipitation at 650 nm, defined as the maximum increase in absorbance (ΔA_{650}) per minute, was calculated within the interval between 0 and 1.0 in absorbance at 650 nm.

2.11. Kinetics of DTNB Reduction. Reduced SpTrx WT and mutants were prepared by adding DTT to a final concentration of 5 mM. The reaction mixture, with SpTrx at a concentration of 0.4 μM and varying DTNB concentrations (ranging from 50 to 200 μM), was incubated at 25 °C for 10 s in buffer G (50 mM MOPS-NaOH, pH 7.0, and 1 mM EDTA). The formation of TNB was monitored by measuring the increase in absorbance at 412 nm. To calculate TNB concentrations, we used an extinction coefficient of 28,300 M^{-1} cm^{-1}, considering that two TNB molecules were formed per reduced DTNB. The Michaelis–Menten constant (K_m) and catalytic rate constant (k_{cat}) were determined from the Lineweaver–Burk plot using GraphPad Prism software.

2.12. Molecular Dynamics (MD) Simulation. The MD simulations of the SpTrx protein variants were performed using Maestro 12.0 (Schrödinger, LLC, New York, NY). The OPLS4 force field,[37] SPC solvent model,[38] were employed to define energetic parameters for all interactions. The proteins were prepared by removing the water molecules and optimizing the structures using the protein preparation wizard. To maintain an electrically neutral state, ions were added as needed by replacing water molecules. Energy minimization was conducted for 1000 steps, ensuring the absence of steric clashes or geometric issues. Solvent molecules were equilibrated with the fixed protein at a temperature of 300 K. The MD simulation was performed at BioCode Ltd. (Liverpool, Merseyside, U.K.) at 200 ns in the NPT ensemble with a 2 fs time step. The RMSD calculations were based on C_α-atoms across all trajectories up to 200 ns and smoothed by Origin Pro, while the RMSF of C_α-atoms at 300 K was estimated over the equilibrated trajectories.

3. RESULTS

3.1. Expression and Purification of Recombinant SpTrx and EcTrx Proteins. Recombinant SpTrx (107 amino acids) and EcTrx (108 amino acids) proteins, including WT and mutants, each with a C-terminal 6× His-tag, were expressed as soluble proteins in *E. coli* BL21 (DE3). Following HisTrap nickel-chelate affinity and Capto Q anion-exchange chromatography, both SpTrx and EcTrx proteins were successfully purified, resulting in 13 kDa monomers in solution (Figure S1), aligning with findings from previous studies.[11,39]

3.2. Thermal Stability of SpTrx WT and Mutants. We evaluated the impact of temperature on the tertiary structure of SpTrx using temperature-induced protein fluorescence. Overall, the emission peak positions of the proteins remained stable up to 60 °C (Figure 2A–F), indicating the preservation of their tertiary structures within the 4–60 °C range. Beyond 60 °C, a noticeable red shift in fluorescence emission maxima occurred, accompanied by increased intensity, suggesting protein unfolding.[40,41] This red shift was substantial (10 nm) in WT, A65T, and W11F/A65T/F69Y, while W11F, W11F/A65T, and W11F/F69Y showed a smaller red shift (4–6 nm), suggesting possible protein aggregation.[40]

Both WT and A65T (Trp-Phe pair) retained their tertiary structures at 70 °C but denatured more cooperatively at 80 °C (Figure 2A,C). W11F/A65T (Phe-Phe pair) completely denatured at 70 °C (Figure 2D). In contrast, W11F (Phe-Phe pair), W11F/F69Y, and W11F/A65T/F69Y (both featuring Phe-Tyr pairs) preserved 50% of their tertiary structures after incubation at 70 °C (Figure 2B,E,F). Between 4 and 60 °C, the structural stabilities of WT and mutants were similar. However, at 70 °C, the order of stability was WT ≈ A65T > W11F/F69Y ≈ W11F/A65T/F69Y ≈ W11F > W11F/A65T (Figure 2G). These results suggest that smaller aromatic pairs (Phe-Phe and Phe-Tyr) are less favorable for SpTrx's thermal stability and tertiary structure.

3.3. T_m Value Analysis. We conducted SYPRO Orange-based thermal shift analysis to determine the T_m values of SpTrx WT and mutants (Table 1 and Figure 2H). WT (Trp-Phe pair) exhibited a T_m of 73.4 °C. In contrast, mutants with smaller aromatic pairs, W11F (Phe-Phe pair) and W11F/F69Y (Phe-Tyr pair), showed lower T_m values of 69.4 and 70.1 °C, respectively. Furthermore, we observed variations in the effect of the Asp8-Thr65 hydrogen bond on T_m values, depending on aromatic pairings. A65T had a similar T_m value (73.4 °C) to the WT. However, there was a significant 5 °C difference between W11F/A65T (Phe-Phe pair) and W11F/A65T/F69Y (Phe-Tyr pair) mutants, with T_m values of 67.4 and 72.9 °C, respectively. This indicates that Thr65's proximity influences the pairing of smaller aromatic residues, particularly affecting the more hydrophobic Phe-Phe pair compared to the Phe-Tyr pair. Moreover, the triple mutant W11F/A65T/F69Y exhibited a T_m value 2.8 °C higher than that of the W11F/F69Y double mutant (70.1 °C), highlighting the stabilizing role of the Thr65-mediated hydrogen bond in the Phe-Tyr pair.

Table 1. T_m Values of SpTrx WT and Mutants

	T_m (°C)	ΔT_m (°C)[a]	ref
WT	73.9 ± 0.0	0	this study
W11F	69.4 ± 0.0	−4.5	
A65T	73.4 ± 0.1	−0.5	
F69Y	74.0 ± 0.1	0.1	11
W11F/A65T	67.4 ± 0.3	−6.5	this study
W11F/F69Y	70.1 ± 0.3	−3.8	
W11F/A65T/F69Y	72.9 ± 0.2	−1.0	

[a]ΔT_m represents the changes in T_m values, calculated as $\Delta T_m = T_m$ (mutants) − T_m (WT). Data presented are the mean ± SD of three independent biological replicates.

https://doi.org/10.1021/acsomega.3c09806
ACS Omega 2024, 9, 10812–10824

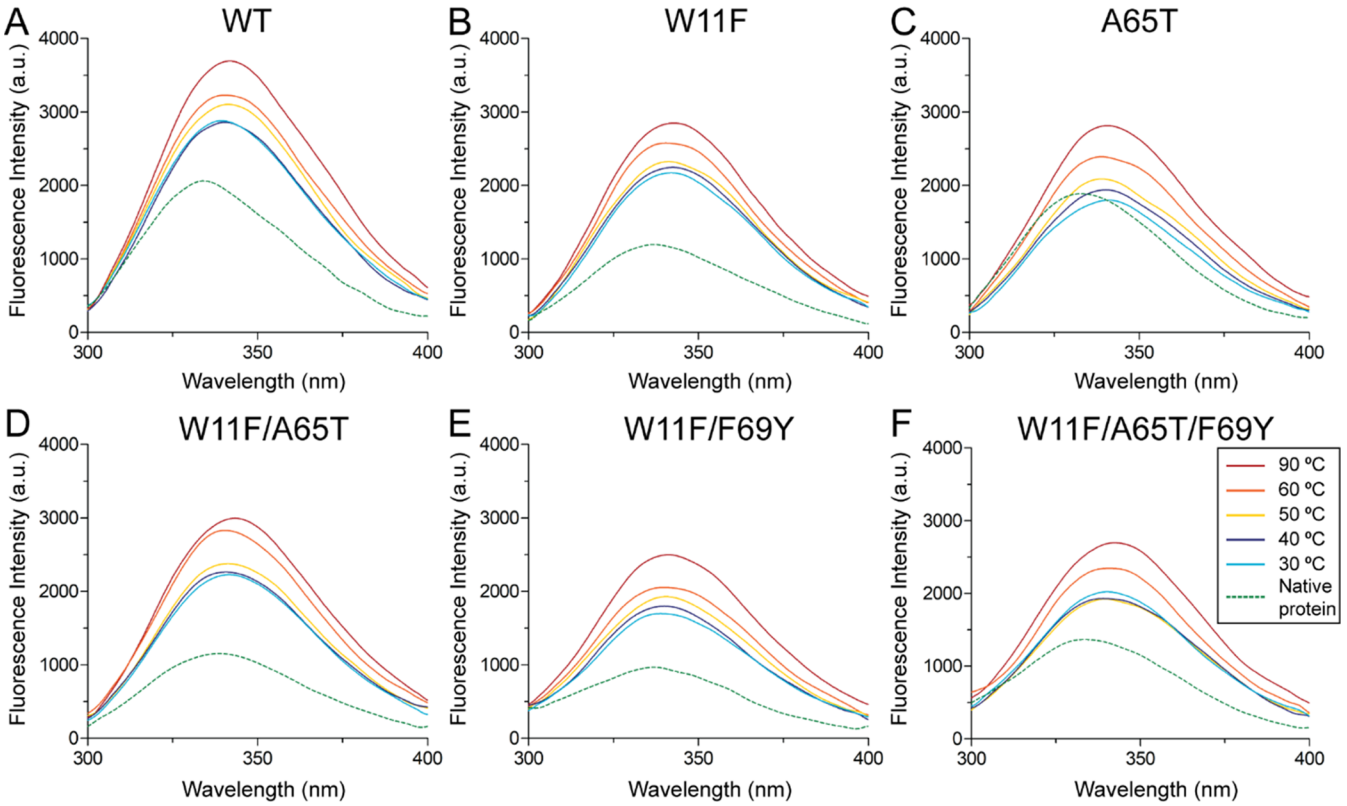

Figure 3. Thermal reversibility of SpTrx WT and mutants. Protein refolding began with incubation at 90 °C, followed by shifting to 60 °C and then cooling in 10 °C decrements until reaching 30 °C, with a 30 min equilibration at each temperature. Panels (A−F) depict the fluorescence spectra during the refolding process at 90 °C (red), 60 °C (orange), 50 °C (yellow), 40 °C (blue), and 30 °C (cyan). The intrinsic fluorescence of each protein at 4 °C (represented by the dashed green line) was measured to determine the native conformation. Data presented represent the means of at least three independent biological replicates.

These results suggest that, based on temperature-induced protein unfolding and thermal shift analysis, a larger aromatic pair is favored for SpTrx's thermal stability. However, the Asp8-Thr65 hydrogen bond behaves differently, strengthening with the Phe-Tyr pair, weakening with the larger Trp-Phe pair, but adversely affecting the smaller Phe-Phe pair.

3.4. Thermal Reversibility Assessment. We evaluated the refolding of SpTrx WT and mutants after thermal unfolding at 90 °C for 30 min, using Trp fluorescence (Figure 3A−F). After gradually cooling from 60 to 30 °C in 10 °C steps for 30 min, SpTrx WT and mutants showed the recovery of their tertiary structure, with reduced fluorescence at 60 °C. However, at 30 °C, their fluorescence levels differed from the native proteins, indicating intermediate states between native and denatured states. Particularly, refolding of the Phe-Phe pairs (W11F, W11F/A65T) was less efficient compared to the Phe-Tyr (W11F/F69Y, W11F/A65T/F69Y) or Trp-Phe pairs (WT, A65T). The A65T mutant exhibited fluorescence similar to the native protein after refolding at 30 °C (Figure 3C), indicating thermal reversibility. Nonetheless, the 10 nm red shift in refolded A65T suggested a distinct conformation from the native protein. These results suggest that the Asp8-Thr65 hydrogen bond in SpTrx contributes to the protein's refolding following temperature-induced unfolding.

3.5. Changes in the Secondary and Tertiary Structures. The effect of aromatic pairings on the secondary and tertiary structures of SpTrx WT and mutants was examined using far-UV CD spectroscopy and bis-ANS fluorescence, respectively (Figure 4). While the substitutions of aromatic residues had no significant effect on the protein's secondary structure (Table S2 and Figure 4A), distinct bis-ANS fluorescence spectra were observed based on specific aromatic pairs (Figure 4B). At 4 °C, W11F (Phe-Phe pair) exhibited significantly higher fluorescence, showing 2.2- and 3.5-fold increase compared to WT (Trp-Phe pair) and W11F/F69Y (Phe-Tyr pair), respectively. This indicates enhanced bis-ANS binding to the exposed hydrophobic region in the native protein.[42] At 50 °C, both WT and W11F/F69Y showed a slight increase in fluorescence intensity compared to their levels at 4 °C, likely due to temperature-induced exposure of the hydrophobic region.[43,44] However, at 50 °C, the fluorescence of W11F significantly decreased, resembling the WT level, indicating hindered bis-ANS binding caused by aggregation.[45] These findings suggest that the preference for the Trp-Phe pair in SpTrx is driven by its larger size, while the presence of the Phe-Phe pair leads to protein structure destabilization and aggregate formation.

3.6. Thermodynamic Stability Analysis. The thermodynamic stability of SpTrx WT and mutants was assessed by measuring urea-induced protein unfolding using fluorescence spectroscopy at 25 °C (Figure 5). Upon exposure to urea, SpTrx WT and A65T (both with Trp-Phe pair) exhibited the highest stability, with a urea denaturation midpoint of 6.3 M, followed by W11F/A65T/F69Y and W11F/F69Y (both with Phe-Tyr pair). W11F and W11F/A65T (both with Phe-Phe pair) showed the lowest stability, with midpoints of 5.2 and 4.7 M, respectively. To assess their thermodynamic stability in the absence of denaturant, we calculated the unfolding free energy

https://doi.org/10.1021/acsomega.3c09806
ACS Omega 2024, 9, 10812−10824

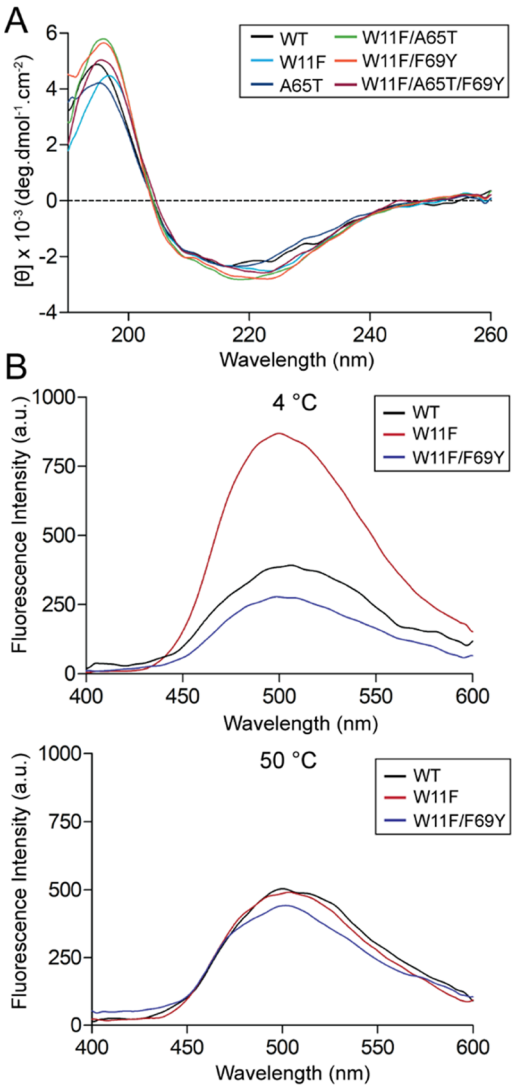

Figure 4. Analysis of secondary and tertiary structures. (A) Far-UV CD spectra of SpTrx WT and mutants at 25 °C. (B) Fluorescence spectra of WT, W11F, and W11F/F69Y. Proteins were preincubated at 4 and 50 °C for 2 h before mixing with bis-ANS. Fluorescence spectra were recorded after a 30 min incubation at 25 °C (excitation at 385 nm). Data presented are the means of at least three independent biological replicates.

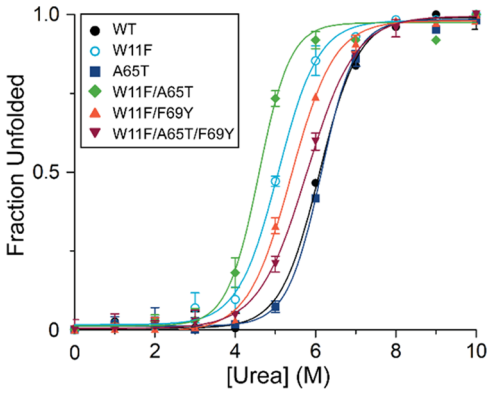

Figure 5. Thermodynamic stability of SpTrx WT and mutants. Urea-induced transitions in Trp fluorescence (Figure S2) were fitted using eq 1 to derive the two-state model of unfolding for each unfolding equilibrium. Data presented are the mean ± SD of at least three independent biological replicates.

($\Delta G^0_{H_2O}$) of SpTrx WT and mutants (Table 2). All mutants displayed a reduction in $\Delta G^0_{H_2O}$, indicating decreased protein stability compared to the WT, especially at lower urea concentrations. The unfolding free energy of these surface aromatic pairs (2−3 kcal/mol) was lower than that of deeply buried single mutations, such as Leu42 and Leu78 (3−5 kcal/mol).[15] Furthermore, all mutants exhibited changes in the m_{NU} values (Table 2), reflecting alterations in the difference in solvent-accessible surface area between the native and denatured states.[46] Our data suggest that mutations from the Trp-Phe pair to either Phe-Tyr or Phe-Phe pairs disrupted the aromatic cluster, resulting in the destabilizing of the α1,α3 interaction.

3.7. Conformational Flexibility Analysis. We assessed the conformational flexibility of different aromatic pairs in SpTrx using acrylamide-induced quenching of intrinsic protein fluorescence (Figure 6A). The acrylamide Stern−Volmer plot indicated that small aromatic pairs exhibited greater flexibility than SpTrx WT, both at 4 and 50 °C. Specifically, W11F and W11F/A65T (both with Phe-Phe pairs) displayed more significant flexibility compared to W11F/F69Y and W11F/A65T/F69Y (both with Phe-Tyr pairs). At 4 °C, the presence of the Asp8-Thr65 hydrogen bond had minimal impact on flexibility. However, at 50 °C, the aromatic pairs without the hydrogen bond showed increased flexibility, as evidenced by higher K_{SV} values (Table 3). These findings indicate that SpTrx with a larger aromatic pair is more rigid than those with a smaller aromatic pair, with the Phe-Phe pair inducing a conformational change associated with higher flexibility compared to the Phe-Tyr pair.

To evaluate the influence of conformational flexibility on protease access to backbone cleavage sites, we exposed SpTrx WT and mutants to trypsin and proteinase K, respectively (Figure S3). A65T exhibited the highest resistance to proteolytic digestion, followed by WT. In contrast, mutants with smaller aromatic pairs were susceptible to proteolytic degradation, while the triple mutant carrying the A65T substitution showed the highest resistance among them (Figure 6B). The Inverse Stern-Vomer constants at 50 °C were plotted against the intensity of native-band fraction of each protein due to nonsynergistic flexibility at 4 °C. Interestingly, the K_{SV}^{-1} values exhibited a correlation with the proportion of the native protein after protease treatment. This correlation further supports the finding that mutants lacking the Asp8-Thr65 hydrogen bond are more flexible and susceptible to proteolytic degradation.

3.8. MD Simulations. We conducted MD simulations of SpTrx WT and mutants to investigate the presence of the Asp8-Thr65 hydrogen bond and its relation with aromatic pairings. C_α-backbone movements were assessed by extracting C_α-RMSD and C_α-RMSF values from the MD trajectory for both WT and mutants (Figure 7). Equilibrium was reached within 50 ns in all proteins (Figure 7A,C). Among them, WT remained the most stable, with a C_α-RMSD average of 2.0 Å and 37% secondary structure content, while W11F exhibited the lowest stability (2.8 Å and 30%) (Table S3 and Figure 7A,C).

C_α-RMSF values showed the most significant change in the α-helix and loop regions, particularly the C-terminal regions of the α2- and α4-helices (residues 26−51 and 90−100), while

https://doi.org/10.1021/acsomega.3c09806
ACS Omega 2024, 9, 10812−10824

Table 2. Thermodynamic Stability Parameters for SpTrx WT and Mutants at pH 7.0 and 25 °C

	$[D]_{1/2}$[a] (M)	m_{NU}[b] (kcal mol^{-1} M^{-1})	$\Delta G^0_{H_2O}$[c] (kcal mol^{-1})	$\Delta\Delta G_{mut}$[d] (kcal mol^{-1})
WT	6.3 ± 0.0	1.27 ± 0.03	7.99 ± 0.18	0
W11F	5.2 ± 0.1	1.00 ± 0.06	5.25 ± 0.27	2.74
A65T	6.3 ± 0.0	1.14 ± 0.04	7.21 ± 0.19	0.78
W11F/A65T	4.7 ± 0.1	1.17 ± 0.04	5.45 ± 0.23	2.54
W11F/F69Y	5.6 ± 0.0	1.02 ± 0.05	5.69 ± 0.28	2.30
W11F/A65T/F69Y	5.9 ± 0.0	0.97 ± 0.06	5.67 ± 0.23	2.32

[a]Urea concentration at the unfolding transition midpoint. [b]Denaturant constant linking free energy and urea concentration. [c]Free energy of unfolding extrapolated to zero denaturants. [d]The change in $\Delta G^0_{H_2O}$ of mutants was given by $\Delta\Delta G_{mut} = \Delta G^0_{H_2OWT} - \Delta G^0_{H_2Omutant}$. Data presented are the mean ± SD of three independent biological replicates.

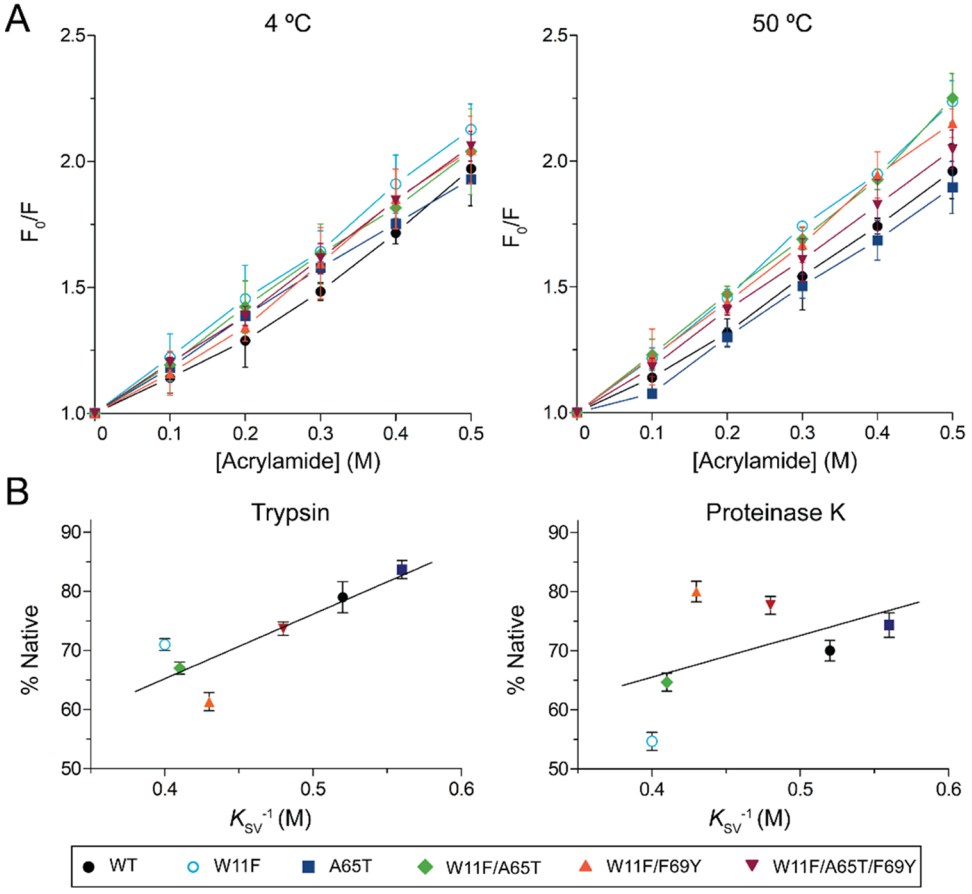

Figure 6. Conformational flexibility of SpTrx WT and mutants. (A) Acrylamide-induced quenching at 4 and 50 °C. Fluorescence intensity changes with acrylamide (0.1−0.5 M) were presented as the ratio of maximum fluorescence intensity without acrylamide (F_0) to that with acrylamide (F). The Stern−Volmer constants (K_{SV}) were calculated using eq 2. (B) Correlation between Inverse Stern−Volmer constant (K_{SV}^{-1}) of Trx mutants at 50 °C and the percentage of native protein resistant to proteolysis by trypsin (left) and proteinase K (right). Data presented are the mean ± SD of three independent biological replicates.

the central β-sheets remained rigid (Figure 7B,D). A65T and W11F/A65T/F69Y mutants exhibited reduced RMSF values attributed to the presence of the Asp-Thr hydrogen bond (residues 6−11 and 66−70), with slightly higher fluctuations observed in W11F/A65T (Figure 7D). On the contrary, the impact of aromatic pairs varied: W11F/F69Y (Phe-Tyr pair) exhibited similar fluctuations to WT (Trp-Phe pair) in α1,α3-helices, whereas W11F (Phe-Phe pair) showed higher fluctuations, up to 2.0 Å compared to WT (Figure 7B). Subsequently, the second half of both β2 and β3-strands, which interact with the loops following both strands, showed increased RMSF values (Figure 7B). These results reveal that significant changes occur in the α-helix and loop regions during cold adaptation, particularly, when a smaller aromatic pair or the Asp-Thr hydrogen bond presents in the α1,α3-helices, leading to destabilization of the α2-helix across the central β-sheet.

3.9. Protein Disulfide Reductase Activity toward Non-Natural Substrates. To assess the protein disulfide reductase activity of SpTrx WT and mutants, we conducted insulin precipitation and DTNB kinetics assays at 25 °C (Table 4 and Figure S4). Insulin reduction-specific activity and catalytic rate for DTNB (k_{cat}^{DTNB}) aligned. WT and A65T (Trp-Phe pair) exhibited the highest reduction activity, while W11F and W11F/A65T (Phe-Phe pair) demonstrated the lowest catalytic activity, which was 30−35% lower than that of WT. In

https://doi.org/10.1021/acsomega.3c09806
ACS Omega 2024, 9, 10812−10824

Table 3. Stern−Volmer Quenching Constant, K_{SV}, and Inverse Stern−Volmer Quenching Constant, K_{SV}^{-1}, of SpTrx WT and Mutants

	4 °C		50 °C		
	K_{SV} (mol^{-1} L)	K_{SV}^{-1} (M)	K_{SV} (mol^{-1} L)	K_{SV}^{-1} (M)	ΔK_{SV}[a] (mol^{-1} L)
WT	1.94 ± 0.34	0.52 ± 0.10	1.93 ± 0.13	0.52 ± 0.03	−0.01[b]
W11F	2.21 ± 0.18	0.45 ± 0.04	2.53 ± 0.12	0.40 ± 0.02	0.32
A65T	1.87 ± 0.10	0.53 ± 0.03	1.79 ± 0.23	0.56 ± 0.05	−0.08[b]
W11F/A65T	2.08 ± 0.17	0.48 ± 0.03	2.50 ± 0.09	0.41 ± 0.06	0.42
W11F/F69Y	2.11 ± 0.25	0.47 ± 0.06	2.37 ± 0.3	0.43 ± 0.05	0.26
W11F/A65T/F69Y	2.13 ± 0.06	0.47 ± 0.01	2.15 ± 0.12	0.48 ± 0.02	0.02

[a]ΔK_{SV} was calculated as the difference between K_{SV} at 50 °C and K_{SV} at 4 °C. Data presented are the mean ± SD of three independent biological replicates. [b]The negative change in ΔK_{SV} value indicated no change in protein conformation.

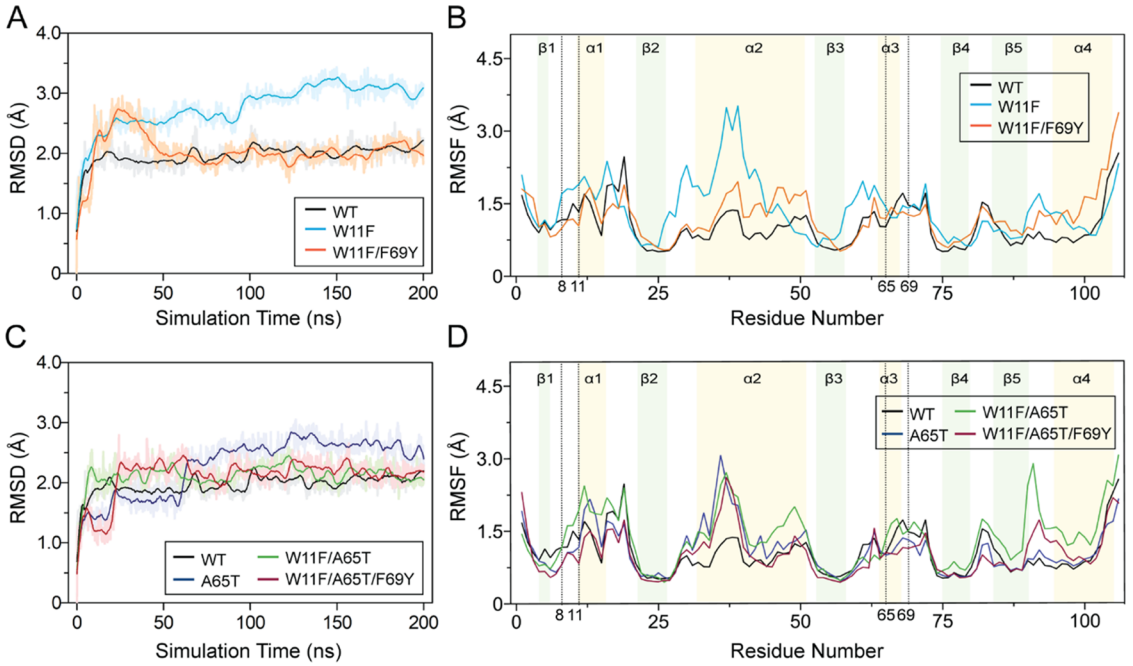

Figure 7. RMSD and RMSF analysis in SpTrx WT and mutants during a 200 ns MD simulation. (A, B) RMSD and RMSF of C_α-atoms in the absence of Thr at position 65. (C, D) RMSD and RMSF of C_α-atoms with Ala65 substituted to Thr, as calculated from the MD simulation trajectory. In SpTrx, residues 8, 11, 65, and 69 are Asp, Trp, Ala, and Phe.

Table 4. Activity of SpTrx WT and Mutants for Non-Natural Substrates at pH 7.0 and 25 °C[a]

	insulin reduction		DTNB kinetics		
	specific activity (ΔA_{650} min^{-1})	relative activity to WT (%)	k_{cat} (s^{-1})	K_m (μM)	relative k_{cat} to WT (%)
WT	2.37 ± 0.08	100	3.54 ± 0.09	150.4 ± 7.2	100
W11F	1.51 ± 0.06	64	2.30 ± 0.07	102.0 ± 7.0	65
A65T	2.16 ± 0.09	91	3.04 ± 0.10	145.6 ± 8.6	86
W11F/A65T	1.62 ± 0.02	68	2.51 ± 0.11	171.7 ± 13.1	71
W11F/F69Y	1.93 ± 0.07	81	2.77 ± 0.09	162.6 ± 9.5	78
W11F/A65T/F69Y	1.66 ± 0.04	70	2.89 ± 0.11	133.1 ± 10.3	82

[a]Data presented are the mean ± SD of three independent biological replicates.

contrast, W11F/F69Y and W11F/A65T/F69Y (Phe-Tyr pair) displayed distinct effects on each substrate. The triple mutant reduced catalytic activity by 30% with insulin but only 18% with DTNB. W11F/F69Y exhibited a 20% reduction in activity with both substrates. DTNB binding affinity appeared largely unaffected by the mutations, except for W11F, which showed a 30% reduction in substrate binding affinity. This decrease may be attributed to a more hydrophobic alteration in the substrate binding site, as observed in the bis-ANS experiment (Figure 4B). These findings highlight the crucial role of maintaining the α1,α3-helices in SpTrx's catalytic activity and substrate binding. Furthermore, the Asp8-Thr65 hydrogen bond reduces SpTrx activity by decreasing the structural flexibility of the α3-helix, as demonstrated in the A65T and triple mutants.

3.10. Effect of Counterpart Mutations on the T_m Values of EcTrx Mutants. To investigate the effect of α1,α3-helix interactions on the thermal stability of EcTrx, we measured the T_m values of EcTrx WT and mutants for comparison with SpTrx (Table 5 and Figure S5). EcTrx WT (Phe-Tyr pair) exhibited a T_m of 80.4 °C. Y70F (Phe-Phe pair)

https://doi.org/10.1021/acsomega.3c09806
ACS Omega 2024, 9, 10812−10824

Table 5. T_m Values of EcTrx WT and Mutants

	T_m (°C)	ΔT_m (°C)[a]
WT	80.4 ± 0.1	0
F12W	79.5 ± 0.1	−0.9
T66A	79.1 ± 0.1	−1.3
Y70F	81.1 ± 0.1	0.7
F12W/Y70F	76.7 ± 0.2	−3.7
T66A/Y70F	79.7 ± 0.1	−0.7
F12W/T66A/Y70F	76.2 ± 0.1	−4.2

[a]Changes in T_m values for mutants compared to the WT: $\Delta T_m = T_m$ (mutants) − T_m (WT). Data presented are the mean ± SD of three independent biological replicates.

showed a minor 0.7 °C increase in the T_m value. However, F12W/Y70F (featuring a larger Trp-Phe pair) exhibited a 3.7 °C decrease (T_m = 76.7 °C) compared to WT.

Disrupting the Asp9-Thr66 hydrogen bond in either Phe-Tyr or Phe-Phe pairs (T66A and T66A/Y70F mutants) led to a 1.4 °C decrease in the T_m values compared to the respective aromatic pair. However, in the Trp-Phe background (F12W/T66A/Y70F), it only led to an insignificant decline. Overall, these differences in T_m values confirm that the presence of a larger aromatic residue hinders the formation of the Asp-Thr hydrogen bond, resulting in weaker hydrogen bonding in EcTrx, whereas pairs with smaller aromatic residues demonstrate stronger hydrogen bonding.

4. DISCUSSION

The Trx-fold is characterized by a stable central β-sheet that has remained conserved throughout evolution.[9,24,25] Hydrophobic interactions between β2 and β4-strands play a pivotal role in the initial folding of Trx.[47] Fragment analysis supports that β2, β3, and β4-strands form the protein's core, contributing to its residual structure in the unfolded state.[13] A buried Phe residue in the β2-strand is crucial for preserving its thermal stability, even in psychrophilic variants.[11,12] Several structural modifications have occurred during the evolution from ancestral Trx to modern-day EcTrx. For instance, the loop connecting the α1-helix and β2-strand in EcTrx is longer compared to that in hyperthermophilic Trx, resulting in a reduction in thermal stability.[28,48,49] Furthermore, the α3-helix in EcTrx becomes more flexible than in LBCA Trx due to the loss of charge−dipole interactions involving Arg88 and the α3-helix, altering dynamics in this region.[22,24,49] Besides the α1,α3 region, the C-terminal α4-helix and β5-strand have also undergone modification with the conversion from salt bridges to hydrophobic interactions, particularly Asp87-Arg101 in ancestral Trxs to Phe102 in EcTrx.[22,24] This sequence-structure-packing change elucidates the robustness of the α4-helix of EcTrx to the amino acid changes with the least effect on the protein structure upon mutation.[39] On the other hand, the folded portion of Trx from *T. thermophilus* showed an overall compact structure than other Trx orthologs.[50] Our study sheds light on the ongoing evolution from mesophilic Trxs to psychrophilic Trxs, emphasizing how the Thr-to-Ala mutation destabilizes the α3-helix, resulting in a larger aromatic pair and reduced packing density, as observed in SpTrx. Conversely, smaller aromatic pairs in SpTrx alter the dynamics of the α2-helix across the central β-sheets, subsequently decreasing enzyme activity.

Interaction analysis using PIC showed notable differences in the distances between aromatic residues in α1,α3-helices, measured from their centers. In LPBCA Trx, Phe11 and Tyr69 were separated by a distance of 5.08 Å, while in EcTrx, the gap between Phe12 and Tyr70 measured 5.85 Å, indicating a reduced packing density. In SpTrx, the bulkiness of Trp11 and Phe69 brought them as close as 5.74 Å. The packing density calculation confirmed this variation, with EcTrx having a packing value of 0.758, while SpTrx exhibited a lower value of 0.751. These results suggest that the aromatic T-shape geometry of the Trp-Phe pair, providing additional energy, compensates for the further decrease in packing density.[51] This packing arrangement within the protein core is considered a driving force behind evolutionary amino acid sequence changes,[50,52] highlighting the significance of the expanded gap between α1 and α3-helices in Trx cold adaptation.

Aromatic residues play distinct roles in enzyme temperature adaptation depending on their positions within the protein structure. When an aromatic residue resides within the protein's interior, its choice between hydrogen bonding and hydrophobic interactions is influenced by the habitat temperature and its interactions with neighboring residues. At hotter and colder temperatures, where the hydrophobicity of aromatic residues weakens,[53,54] Tyr's hydrogen bonding is favored due to its hydroxyl group.[55−59] At intermediate temperatures, bulkier Trp and purely hydrophobic Phe residues become dominant, with Trp engaging in hydrogen bonding through its N−H group and Phe contributing through hydrophobic interactions.[60,61]

However, pairwise aromatic interactions behave differently, especially when located on the protein's surface. In the thermophiles, where thermal stability is crucial, aromatic clusters are predominantly found on the protein surface and tend to be small in size.[62] In Trxs from various temperature environments, the Phe-Tyr pair, known for its aiding in protein folding, enhancing stability, and ensuring proper functionality,[62−65] is the preferred aromatic pair in α1,α3-helices. The presence of a hydrophilic group, such as Tyr hydroxyl or Trp indole group, on the protein surface strengthens the formation of a robust hydration shield,[66] thereby enhancing the stability of the protein structure.[62] Despite the energetically favorable nature of Phe-Phe pair,[67] it represents only an alternative aromatic pairing option.[63] Nevertheless, some psychrophilic Trxs, like PhTrx (*Pseudoalteromonas haloplanktis*), deviate from this preference by incorporating a small Phe-Phe pair alongside an additional Thr residue (Figure 1A). This unique configuration contributes to its compact structure and exceptional thermal stability, boasting a half-life of 4.4 h at 95 °C.[18] This deviation possibly signifies a transitional phase between ancestral Trxs with smaller aromatic pairs and psychrophilic Trxs with larger aromatic pairs. Moreover, when examining the Trp-Tyr pair in EcTrx (F12W) and the Trp-Tyr pair in SpTrx (F69Y),[11] both variants exhibit comparable thermal stability to their respective WT forms (Table 5). These findings suggest that the Trp indole ring and Tyr hydroxyl group can coexist within EcTrx's structure, facilitated by interactions with water molecules. In contrast, the flexible structure of SpTrx allows the formation of a hydrogen bond between Trp and Tyr as a viable alternative (Figure S6).

5. CONCLUSIONS

Our findings suggest that Trx has undergone structural changes to enhance flexibility at colder temperatures, which are characterized by the disruption of the Asp-Thr hydrogen bond in the α1,α3-helices. This disruption promotes the

https://doi.org/10.1021/acsomega.3c09806
ACS Omega 2024, 9, 10812−10824

transition from a smaller aromatic pair to a larger one, resulting in reduced packing density. These insights shed light on the evolutionary processes responsible for Trx's cold adaptation.

■ ASSOCIATED CONTENT

Supporting Information

The Supporting Information is available free of charge at https://pubs.acs.org/doi/10.1021/acsomega.3c09806.

List of PCR primers for site-directed mutagenesis, secondary structure analysis of SpTrx WT and mutants, protein secondary structure elements throughout the MD simulation, SDS-PAGE analysis, urea-induced unfolding transitions monitored by Trp fluorescence, limited proteolysis analyzed by tricine-SDS-PAGE, insulin reduction turbidimetric assay, thermal denaturation curve of EcTrx WT and mutants, and three-dimensional structures of SpTrx WT and mutants with distinct aromatic pairings in α1,α3-helices (PDF)

Accession Codes

• SpTrx: WP_010164143.1 • SgTrx: WP_133186775.1 • SyTrx: WP_188445499.1 • SeTrx: WP_010402847.1 • PaTrx: WP_011281244.1 • PhTrx: WP_008109071.1 • EcTrx: 2TRX • AaTrx: ABI83631.1 • ScTrx: WP_002884315.1 • TtTrx: 2CVK • StTrx: 2E0Q • LBCA: 4BA7 • LPBCA: 2YJ7 • LGPCA: 2YN1

■ AUTHOR INFORMATION

Corresponding Author

ChangWoo Lee − *Department of Biomedical Science and Center for Bio-Nanomaterials, Daegu University, Gyeongsan 38453, South Korea;* orcid.org/0000-0002-0872-4500; Phone: +82-53-850-6464; Email: leec@daegu.ac.kr

Author

Tu Anh Nguyen − *Department of Biomedical Science and Center for Bio-Nanomaterials, Daegu University, Gyeongsan 38453, South Korea*

Complete contact information is available at: https://pubs.acs.org/10.1021/acsomega.3c09806

Author Contributions

T.A.N.: conceptualization, investigation, writing—original draft. C.L.: conceptualization, funding acquisition, writing—original draft, writing—review and editing.

Notes

The authors declare no competing financial interest.

■ ACKNOWLEDGMENTS

This work was supported by the Basic Science Research Program through the National Research Foundation of Korea (NRF) funded by the Ministry of Education (NRF-2018R1D1A3B07048635 to C.L.). The authors thank Chang-Nam Kim (Kyungpook National University) for measuring the CD spectra.

■ ABBREVIATIONS

Bis-ANS, 4,4′-dianilino-1,1′-binaphthyl-5,5′-disulfonic acid dipotassium salt; DTNB, 5,5-dithio-bis(2-nitrobenzoic acid); DTT, dithiothreitol; EDTA, ethylenediaminetetraacetic acid; IPTG, isopropyl β-D-1-thiogalactopyranoside; MOPS, 3-morpholinopropane-1-sulfonic acid; NADPH, β-nicotinamide adenine dinucleotide phosphate hydrogen; RMSD, root-mean-square deviation; RMSF, root-mean-square fluctuation; SDS-PAGE, sodium dodecyl sulfate-polyacrylamide gel electrophoresis; PMSF, phenylmethylsulfonyl fluoride; TNB, thio nitrobenzoic acid; Trx, thioredoxin

■ REFERENCES

(1) Collet, J. F.; Messens, J. Structure, function, and mechanism of thioredoxin proteins. *Antioxid. Redox Signaling* **2010**, *13* (8), 1205−1216.

(2) Holmgren, A.; Soderberg, B. O.; Eklund, H.; Branden, C. I. Three-dimensional structure of *Escherichia coli* thioredoxin-S2 to 2.8 Å resolution. *Proc. Natl. Acad. Sci. U.S.A.* **1975**, *72* (6), 2305−2309.

(3) Katti, S. K.; LeMaster, D. M.; Eklund, H. Crystal structure of thioredoxin from *Escherichia coli* at 1.68 Å resolution. *J. Mol. Biol.* **1990**, *212* (1), 167−184.

(4) Lu, J.; Holmgren, A. The thioredoxin antioxidant system. *Free Radical Biol. Med.* **2014**, *66*, 75−87.

(5) Arnér, E. S. J.; Holmgren, A. Physiological functions of thioredoxin and thioredoxin reductase. *Eur. J. Biochem.* **2000**, *267* (20), 6102−6109.

(6) Napolitano, S.; Reber, R. J.; Rubini, M.; Glockshuber, R. Functional analyses of ancestral thioredoxins provide insights into their evolutionary history. *J. Biol. Chem.* **2019**, *294* (38), 14105−14118.

(7) Tzul, F. O.; Vasilchuk, D.; Makhatadze, G. I. Evidence for the principle of minimal frustration in the evolution of protein folding landscapes. *Proc. Natl. Acad. Sci. U.S.A.* **2017**, *114* (9), E1627−E1632.

(8) Risso, V. A.; Sanchez-Ruiz, J. M.; Ozkan, S. B. Biotechnological and protein-engineering implications of ancestral protein resurrection. *Curr. Opin. Struct. Biol.* **2018**, *51*, 106−115.

(9) Modi, T.; Campitelli, P.; Kazan, I. C.; Ozkan, S. B. Protein folding stability and binding interactions through the lens of evolution: a dynamical perspective. *Curr. Opin. Struct. Biol.* **2021**, *66*, 207−215.

(10) Romero-Romero, M. L.; Risso, V. A.; Martinez-Rodriguez, S.; Ibarra-Molero, B.; Sanchez-Ruiz, J. M. Engineering ancestral protein hyperstability. *Biochem. J.* **2016**, *473* (20), 3611−3620.

(11) Nguyen, T. T.; Hoang, T.; Tran, K. N.; Kim, H.; Jang, S. H.; Lee, C. Essential roles of buried phenylalanine in the structural stability of thioredoxin from a psychrophilic Arctic bacterium *Sphingomonas* sp. *PLoS One* **2021**, *16* (12), No. e0261123.

(12) Assemat, K.; Alzari, P. M.; Clement-Metral, J. Conservative substitutions in the hydrophobic core of *Rhodobacter sphaeroides* thioredoxin produce distinct functional effects. *Protein Sci.* **1995**, *4* (12), 2510−2516.

(13) Bhutani, N.; Udgaonkar, J. B. Folding subdomains of thioredoxin characterized by native-state hydrogen exchange. *Protein Sci.* **2003**, *12* (8), 1719−1731.

(14) Santos, J.; Marino-Buslje, C.; Kleinman, C.; Ermacora, M. R.; Delfino, J. M. Consolidation of the thioredoxin fold by peptide recognition: interaction between *E. coli* thioredoxin fragments 1−93 and 94−108. *Biochemistry* **2007**, *46* (17), 5148−5159.

(15) Hellinga, H. W.; Wynn, R.; Richards, F. M. The hydrophobic core of *Escherichia coli* thioredoxin shows a high tolerance to nonconservative single amino acid substitutions. *Biochemistry* **1992**, *31* (45), 11203−11209.

(16) Cotugno, R.; Ruocco, M. R.; Marco, S.; Falasca, P.; Evangelista, G.; Raimo, G.; Chambery, A.; Di Maro, A.; Masullo, M.; De Vendittis, E. Differential cold-adaptation among protein components of the thioredoxin system in the psychrophilic eubacterium *Pseudoalteromonas haloplanktis* TAC 125. *Mol. Biosyst.* **2009**, *5* (5), 519−528.

(17) Pedone, E.; Cannio, R.; Saviano, M.; Rossi, M.; Bartolucci, S. Prediction and experimental testing of *Bacillus acidocaldarius* thioredoxin stability. *Biochem. J.* **1999**, *339* (2), 309−317.

(18) Falasca, P.; Evangelista, G.; Cotugno, R.; Marco, S.; Masullo, M.; De Vendittis, E.; Raimo, G. Properties of the endogenous components of the thioredoxin system in the psychrophilic

eubacterium *Pseudoalteromonas haloplanktis* TAC 125. *Extremophiles* **2012**, *16* (3), 539−552.
(19) Sahtout, N.; Kuttiyatveetil, J. R. A.; Sanders, D. A. R. Structure and function of the putative thioredoxin 1 from the thermophilic eubacterium *Thermosipho africanus* strain TCF52B. *Biochim. Biophys. Acta, Proteins Proteomics* **2019**, *1867* (4), 426−433.
(20) Perez-Jimenez, R.; Li, J.; Kosuri, P.; Sanchez-Romero, I.; Wiita, A. P.; Rodriguez-Larrea, D.; Chueca, A.; Holmgren, A.; Miranda-Vizuete, A.; Becker, K.; et al. Diversity of chemical mechanisms in thioredoxin catalysis revealed by single-molecule force spectroscopy. *Nat. Struct. Mol. Biol.* **2009**, *16* (8), 890−896.
(21) Psenakova, K.; Hexnerova, R.; Srb, P.; Obsilova, V.; Veverka, V.; Obsil, T. The redox-active site of thioredoxin is directly involved in apoptosis signal-regulating kinase 1 binding that is modulated by oxidative stress. *FEBS J.* **2020**, *287* (8), 1626−1644.
(22) Cabrera, Á. C.; Sanchez-Murcia, P. A.; Gago, F. Making sense of the past: hyperstability of ancestral thioredoxins explained by free energy simulations. *Phys. Chem. Chem. Phys.* **2017**, *19* (34), 23239−23246.
(23) Mancusso, R.; Cruz, E.; Cataldi, M.; Mendoza, C.; Fuchs, J.; Wang, H.; Yang, X.; Tasayco, M. L. Reversal of negative charges on the surface of *Escherichia coli* thioredoxin: pockets versus protrusions. *Biochemistry* **2004**, *43* (13), 3835−3843.
(24) Modi, T.; Huihui, J.; Ghosh, K.; Ozkan, S. B. Ancient thioredoxins evolved to modern-day stability-function requirement by altering native state ensemble. *Philos. Trans. R. Soc., B* **2018**, *373* (1749), No. 20170184.
(25) Campitelli, P.; Modi, T.; Kumar, S.; Ozkan, S. B. The role of conformational dynamics and allostery in modulating protein evolution. *Annu. Rev. Biophys.* **2020**, *49*, 267−288.
(26) Lee, H.; Shin, S. C.; Lee, J.; Kim, S. J.; Kim, B. K.; Hong, S. G.; Kim, E. H.; Park, H. Genome sequence of *Sphingomonas* sp. strain PAMC 26621, an Arctic-lichen-associated bacterium isolated from a *Cetraria* sp. *J. Bacteriol.* **2012**, *194* (11), No. 3030.
(27) Mirdita, M.; Schutze, K.; Moriwaki, Y.; Heo, L.; Ovchinnikov, S.; Steinegger, M. ColabFold: making protein folding accessible to all. *Nat. Methods* **2022**, *19* (6), 679−682.
(28) Ingles-Prieto, A.; Ibarra-Molero, B.; Delgado-Delgado, A.; Perez-Jimenez, R.; Fernandez, J. M.; Gaucher, E. A.; Sanchez-Ruiz, J. M.; Gavira, J. A. Conservation of protein structure over four billion years. *Structure* **2013**, *21* (9), 1690−1697.
(29) Sievers, F.; Wilm, A.; Dineen, D.; Gibson, T. J.; Karplus, K.; Li, W.; Lopez, R.; McWilliam, H.; Remmert, M.; Soding, J.; et al. Fast, scalable generation of high-quality protein multiple sequence alignments using Clustal Omega. *Mol. Syst. Biol.* **2011**, *7*, No. 539.
(30) Tina, K. G.; Bhadra, R.; Srinivasan, N. PIC: Protein Interactions Calculator. *Nucleic Acids Res.* **2007**, *35* (2), W473−W476.
(31) Chen, C. R.; Makhatadze, G. I. ProteinVolume: calculating molecular van der waals and void volumes in proteins. *BMC Bioinf.* **2015**, *16* (1), No. 101.
(32) Creighton, T. E. *Protein Structure: A Practical Approach*; IRL Press at Oxford University Press, 1997.
(33) Lehrer, S. S. Solute perturbation of protein fluorescence. The quenching of the tryptophyl fluorescence of model compounds and of lysozyme by iodide ion. *Biochemistry* **1971**, *10* (17), 3254−3263.
(34) Schägger, H. Tricine-SDS-PAGE. *Nat. Protoc.* **2006**, *1* (1), 16−22.
(35) Schneider, C. A.; Rasband, W. S.; Eliceiri, K. W. NIH Image to ImageJ: 25 years of image analysis. *Nat. Methods* **2012**, *9* (7), 671−675.
(36) Micsonai, A.; Moussong, E.; Wien, F.; Boros, E.; Vadaszi, H.; Murvai, N.; Lee, Y. H.; Molnar, T.; Refregiers, M.; Goto, Y.; et al. BeStSel: webserver for secondary structure and fold prediction for protein CD spectroscopy. *Nucleic Acids Res.* **2022**, *50* (W1), W90−W98.
(37) Lu, C.; Wu, C.; Ghoreishi, D.; Chen, W.; Wang, L.; Damm, W.; Ross, G. A.; Dahlgren, M. K.; Russell, E.; Von Bargen, C. D.; et al. OPLS4: improving force field accuracy on challenging regimes of chemical space. *J. Chem. Theory Comput.* **2021**, *17* (7), 4291−4300.
(38) Frank, H. S.; Wen, W.-Y. Ion-solvent interaction. Structural aspects of ion-solvent interaction in aqueous solutions: a suggested picture of water structure. *Discuss. Faraday Soc.* **1957**, *24* (0), 133−140.
(39) Noguera, M. E.; Vazquez, D. S.; Ferrer-Sueta, G.; Agudelo, W. A.; Howard, E.; Rasia, R. M.; Manta, B.; Cousido-Siah, A.; Mitschler, A.; Podjarny, A.; Santos, J. Structural variability of *E. coli* thioredoxin captured in the crystal structures of single-point mutants. *Sci. Rep.* **2017**, *7*, No. 42343.
(40) Duy, C.; Fitter, J. How aggregation and conformational scrambling of unfolded states govern fluorescence emission spectra. *Biophys. J.* **2006**, *90* (10), 3704−3711.
(41) Saha, P.; Manna, C.; Chakrabarti, J.; Ghosh, M. Reversible thermal unfolding of a yfdX protein with chaperone-like activity. *Sci. Rep.* **2016**, *6*, No. 29541.
(42) Gabellieri, E.; Strambini, G. B. ANS fluorescence detects widespread perturbations of protein tertiary structure in ice. *Biophys. J.* **2006**, *90* (9), 3239−3245.
(43) Das, K. P.; Surewicz, W. K. Temperature-induced exposure of hydrophobic surfaces and its effect on the chaperone activity of α-crystallin. *FEBS Lett.* **1995**, *369* (2−3), 321−325.
(44) Raman, B.; Ramakrishna, T.; Rao, C. M. Temperature dependent chaperone-like activity of α-crystallin. *FEBS Lett.* **1995**, *365* (2−3), 133−136.
(45) Tran, T. V.; Hoang, T.; Jang, S. H.; Lee, C. Unraveling the roles of aromatic cluster side-chain interactions on the structural stability and functional significance of psychrophilic *Sphingomonas* sp. glutaredoxin 3. *PLoS One* **2023**, *18* (8), No. e0290686.
(46) Dill, K. A.; Shortle, D. Denatured states of proteins. *Annu. Rev. Biochem.* **1991**, *60*, 795−825.
(47) Tasayco, M. L.; Fuchs, J.; Yang, X. M.; Dyalram, D.; Georgescu, R. E. Interaction between two discontiguous chain segments from the β-sheet of *Escherichia coli* thioredoxin suggests an initiation site for folding. *Biochemistry* **2000**, *39* (35), 10613−10618.
(48) Esposito, L.; Ruggiero, A.; Masullo, M.; Ruocco, M. R.; Lamberti, A.; Arcari, P.; Zagari, A.; Vitagliano, L. Crystallographic and spectroscopic characterizations of *Sulfolobus solfataricus* TrxA1 provide insights into the determinants of thioredoxin fold stability. *J. Struct. Biol.* **2012**, *177* (2), 506−512.
(49) Ruggiero, A.; Smaldone, G.; Esposito, L.; Balasco, N.; Vitagliano, L. Loop size optimization induces a strong thermal stabilization of the thioredoxin fold. *FEBS J.* **2019**, *286* (9), 1752−1764.
(50) Rehse, P. H.; Kumei, M.; Tahirov, T. H. Compact reduced thioredoxin structure from the thermophilic bacteria *Thermus thermophilus*. *Proteins* **2005**, *61* (4), 1032−1037.
(51) Makwana, K. M.; Mahalakshmi, R. Comparative analysis of cross strand aromatic-Phe interactions in designed peptide β-hairpins. *Org. Biomol. Chem.* **2014**, *12* (13), 2053−2061.
(52) Chen, J.; Stites, W. E. Packing is a key selection factor in the evolution of protein hydrophobic cores. *Biochemistry* **2001**, *40* (50), 15280−15289.
(53) Dias, C. L.; Ala-Nissila, T.; Wong-ekkabut, J.; Vattulainen, I.; Grant, M.; Karttunen, M. The hydrophobic effect and its role in cold denaturation. *Cryobiology* **2010**, *60* (1), 91−99.
(54) van Dijk, E.; Hoogeveen, A.; Abeln, S. The hydrophobic temperature dependence of amino acids directly calculated from protein structures. *PLoS Comput. Biol.* **2015**, *11* (5), No. e1004277.
(55) Kashif, A.; Tran, L. H.; Jang, S. H.; Lee, C. Roles of active-site aromatic residues in cold adaptation of *Sphingomonas glacialis* esterase EstSP1. *ACS Omega* **2017**, *2* (12), 8760−8769.
(56) Lee, Y.; Kwak, C.; Jeong, K. W.; Durai, P.; Ryu, K. S.; Kim, E. H.; Cheong, C.; Ahn, H. C.; Kim, H. J.; Kim, Y. Tyr51: key determinant of the low thermostability of the *Colwellia psychrerythraea* cold-shock protein. *Biochemistry* **2018**, *57* (26), 3625−3640.
(57) Nguyen, T. A.; Jang, S. H.; Lee, C. C-terminal β8-α9 interaction modulates thermal stability and enzymatic activity

https://doi.org/10.1021/acsomega.3c09806
ACS Omega 2024, 9, 10812−10824

differently in hyperthermophilic esterase EstE1 and mesophilic esterase rPPE. *Appl. Environ. Microbiol.* **2023**, *89* (6), No. e0066223.
(58) Truongvan, N.; Jang, S. H.; Lee, C. Flexibility and stability trade-off in active site of cold-adapted *Pseudomonas mandelii* esterase EstK. *Biochemistry* **2016**, *55* (25), 3542−3549.
(59) Van Tran, T.; Nguyen, H.; Vu, L.; Lee, C. Structural conservation in the glutathione binding in *Sphingomonas* sp. glutaredoxin Grx3 and variations for cold adaptation. *Biochim. Biophys. Acta, Proteins Proteomics* **2024**, *1872* (1), No. 140971.
(60) Boyineni, J.; Kim, J.; Kang, B. S.; Lee, C.; Jang, S. H. Enhanced catalytic site thermal stability of cold-adapted esterase EstK by a W208Y mutation. *Biochim. Biophys. Acta, Proteins Proteomics* **2014**, *1844* (6), 1076−1082.
(61) Tran, K. N.; Jang, S. H.; Lee, C. Effect of active-site aromatic residues Tyr or Phe on activity and stability of glucose 6-phosphate dehydrogenase from psychrophilic Arctic bacterium *Sphingomonas* sp. *Biochim. Biophys. Acta, Proteins Proteomics* **2021**, *1869* (1), No. 140543.
(62) Kannan, N.; Vishveshwara, S. Aromatic clusters: a determinant of thermal stability of thermophilic proteins. *Protein Eng., Des. Sel.* **2000**, *13* (11), 753−761.
(63) Anjana, R.; Vaishnavi, M. K.; Sherlin, D.; Kumar, S. P.; Naveen, K.; Kanth, P. S.; Sekar, K. Aromatic-aromatic interactions in structures of proteins and protein-DNA complexes: a study based on orientation and distance. *Bioinformation* **2012**, *8* (24), 1220−1224.
(64) Serrano, L.; Bycroft, M.; Fersht, A. R. Aromatic-aromatic interactions and protein stability. Investigation by double-mutant cycles. *J. Mol. Biol.* **1991**, *218* (2), 465−475.
(65) Bunik, V.; Raddatz, G.; Lemaire, S.; Meyer, Y.; Jacquot, J. P.; Bisswanger, H. Interaction of thioredoxins with target proteins: role of particular structural elements and electrostatic properties of thioredoxins in their interplay with 2-oxoacid dehydrogenase complexes. *Protein Sci.* **1999**, *8* (1), 65−74.
(66) Sterpone, F.; Bertonati, C.; Briganti, G.; Melchionna, S. Key role of proximal water in regulating thermostable proteins. *J. Phys. Chem. B* **2009**, *113* (1), 131−137.
(67) Butterfield, S. M.; Patel, P. R.; Waters, M. L. Contribution of aromatic interactions to α-helix stability. *J. Am. Chem. Soc.* **2002**, *124* (33), 9751−9755.

https://doi.org/10.1021/acsomega.3c09806
ACS Omega 2024, 9, 10812−10824